Flow over a slot-perforated flat surface between two parallel plates

Shuichi Torii
Department of Mechanical Engineering, Kagoshima University, Kagoshima, Japan
Wen-Jei Yang
Department of Mechanical Engineering and Applied Mechanics, University of Michigan, Ann Arbor, Michigan, USA and
Shinzaburo Umeda
Department of Civil Engineering, Fukuyama University, Fukuyama, Hiroshima, Japan

Keywords *Flow, Numerical simulation, Plate*

Abstract *A theoretical and experimental study is performed to investigate unsteady, two-dimensional, incompressible fluid flow over both sides of a slot-perforated flat surface, which is placed in a two-dimensional channel. The governing boundary-layer equations are discretized by means of a finite-difference technique to determine streamwise and transverse velocity components. The roles of both the Reynolds number and the ratio of the slot width, d, to the plate thickness, δ, on the velocity field are disclosed. It is found from the study that: (i) the flow pattern between two plates can be classified into four categories depending on a combination of Re and d/δ, (ii) at a small value of Re and/or d/δ, flow over the slot exhibits no timewise variation, (iii) when Re and d/δ exceed certain values, an alternate crossing of flow from one side of the plate to the other occurs across the slot, and (iv) a further increase in Re results in a complex flow both inside the slot and on the plate downstream of the slot. These results are confirmed by the flow visualization using ion-exchange resins.*

Nomenclature

B = channel length, m
d = slot width, m
L = length of plate, m
P = pressure, Pa
Re = Reynolds number, $u_m\delta/v$
t = time, second
U,V, = velocity components in streamwise and transverse directions, respectively, m/s
u_m = axial mean velocity over whole channel cross-section, m/s
x, y = coordinate, m
ΔX, ΔY = mesh size, m
W = channel width, m
ρ = density, kg/m^3
v = molecular viscosity, m^2/s
δ = plate thickness, m

Subscripts

in = inlet
w = wall

Introduction

The heat exchanger is an essential unit in heat extraction and recovery systems. With increasing emphasis on economic and energy saving considerations, a great deal of research effort is devoted to developing more efficient heat-transfer surfaces. In the design of advanced heat exchangers, louver-fins, strip-fins, wavy-fins and perforated-fins are widely used to achieve high heat transfer

International Journal of Numerical Methods for Heat & Fluid Flow, Vol. 9 No. 2, 1999, pp. 136-150,

efficiency and compactness. A comparison of performances among these surfaces was made by Wong *et al.* (1971). Kays (1958) reported that perforation results in a substantial increase in heat-transfer performance without introducing a pronounced form drag. Perforated fin tubular heat exchangers may be made either in small size and light weight as air-cooled condensers or in large size as air-cooled heat exchangers. This viewpoint was supported by some investigators (Shah and Osborn, 1967; Wong *et al.,* 1971).

Perforated plates may be employed as an extended surface for internal cooling of turbine blades, because the perforated-plate-fin surface is compact and induces high heat-transfer performance by boundary layer interruption due to perforations without the salient penalty of the form drag. There are two kinds of flow associated with perforated plates; one is parallel and the other normal to the plate. Flows parallel to the perforated plates were used in dry cooling towers (Liang *et al.,* 1974), air-cooled condensers for Rankine cycle engines (Wong *et al.,* 1971), and gas turbine recuperators (Siegla, 1972). Flows normal to plate surfaces were applied in heat exchanger devices for air separation (McMahon *et al.,* 1950), helium liquefaction and refrigeration (Vonk, 1968), and Claude-cycle cryogenic refrigerations (Fleming, 1969). Liang and Yang (1975a,b), Liang *et al.* (1977), and Lee and Yang (1978) conducted a series of studies on the perforated surfaces and disclosed that flow transition can be promoted by perforation. Their heat-transfer performance was found to be superior to the non-perforated case in the transitional and turbulent flow regimes under the same pressure drop or friction power. Fujii *et al.* (1988) used plates with trapezoidal-shape perforations to enhance the secondary flow through suction and injection. Hwang *et al.* (1996) investigated the effects of perforation geometry, flow angle aspect ratio, and the ratio of channel length to hole diameter on heat transfer performance. It was found that:

(1) the perforation induces transition from laminar to turbulent flow;

(2) the effect of the ratio of channel length to hole diameter is dominant; and

(3) a high pitch noise is produced in the transitional flow regime.

These studies indicate that perforation induces an amplification in heat transfer performance. Only a few investigations have been directed toward understanding basic flow mechanisms: Liang and Yang (1975c) investigated the flow characteristics and the mechanisms of plate vibration and noise, induced by the shedding of vortices from perforated holes. They employed a combined holographic and strain-gage technique with the flow visualization method using dye injection, and revealed that frequency jumps and vigorous plate vibrations, accompanied by acute noise in the turbulent flow regime, were caused by acoustical lock-in phenomena. Later, Liang (1975) and Liang *et al.* (1976) studied the effects of geometry and arrangement of the perforations on fluid flow behavior by visualizing streak-lines in the flow with dye-injection technique. It was found that the ratio of slot length in the flow direction to its thickness plays a very important role in flow behavior. A corresponding numerical analysis was

performed to investigate the effects of both the Reynolds number and the ratio of the slot width, d, to the plate thickness, δ, on the velocity field (Torii and Yang 1998). They reported that the calculation reproduces the unsteady-state fluid transport phenomena over both sides of the single-plate-single-slot, which are reported by Liang (1975), and the flow pattern between two plates placed in free stream can be classified into four categories depending on a combination of Re and d/δ. Although numerical simulation provides detailed information on the transport phenomena, the existing theoretical and experimental study is confined to the fluid flow over the perforated plate in free stream. Thus no information on these fluid flow transport characteristics gives the design of the industrial applications, i.e., advanced heat exchangers, because the perforated surfaces are installed in the channel.

The present study deals with numerical visualization of flow over both sides of a slot-perforated surface which is placed in the two-dimensional channel. The governing differential equations for two-dimensional unsteady flow are discretized by means of a finite-difference technique. Theoretical predictions are tested with experiments employing flow visualization methods.

Experimental apparatus and procedure

Figure 1 depicts the test setup employed in the present study. It consists of an upper (supply) tank and a lower (receiving) tank with a test section placed in between both tanks. The test fluid, water, is circulated using a pump with flow rates regulated by a valve for adjusting the liquid level in the upper tank, Hu. In the test section, a slot-perforated plate with a length of L=25 mm and a thickness of δ=10 mm is installed in the water channel, which is 20 mm deep, 25 mm wide, and 300 mm long (in the flow direction). An acryl plate is placed on top of the channel as a cover for observation and illumination. The liquid level in the upper tank, Hu, is varied to change the Reynolds number, Re. The plate length, L, and its thickness, δ, are fixed, i.e., L/δ = 2.5, and only the slot width, d, is varied to investigate the effect of perforation geometry on the flow behavior. Flow rate was measured in each test, through which the Reynolds number was determined. Flow visualization was performed using ion exchange resins (highly-porous polymer particles) as the tracer. The flow patterns over the slot-perforated plates were recorded in still photographs, which were taken at the region marked in Figure 1. The ranges of the parameters are Reynolds numbers Re=30 ~ 400, and the ratios of the slot width to the plate thickness d/δ=2.0 ~ 5.0.

Numerical simulation

The proposed physical model to be studied is schematically illustrated in Figure 2. A single-slot perforated surface placed in a two-dimensional channel consists of two plain straight plates (i.e. the front and rear plates), of length, L, and thickness,δ, aligned in the flow direction with a spacing of d. The isothermal, laminar flow field is governed by the unsteady two-dimensional, incompressible Navier-Stokes equations with the continuity equation. Under the assumptions of constant physical properties, the simplified conservation equations for mass and momentum read:

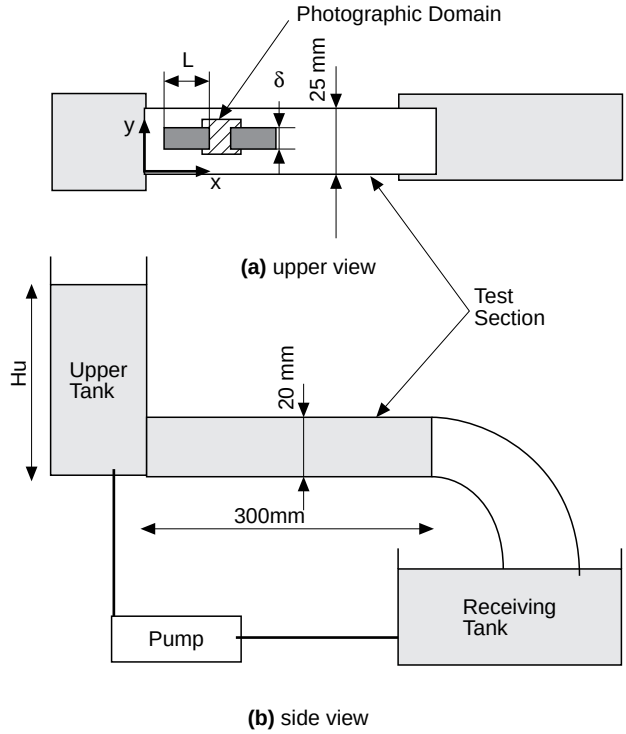

Figure 1.
A schematic of the experimental apparatus

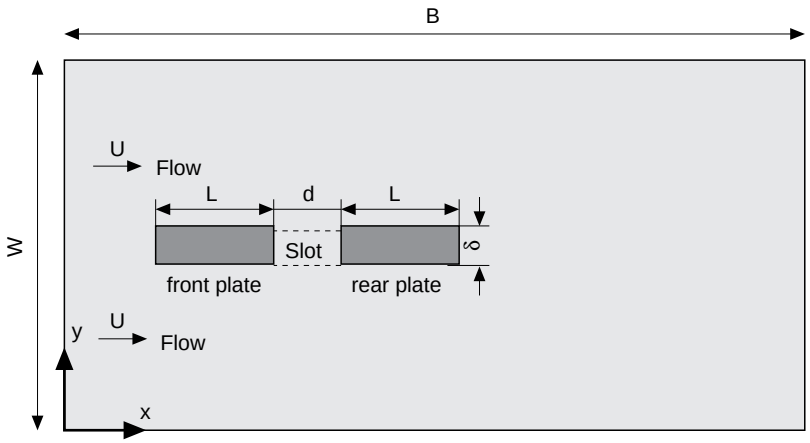

Figure 2.
A schematic of the physical system and coordinate

$$\frac{\partial U}{\partial x} + \frac{\partial V}{\partial y} = 0 \ , \tag{1}$$

and

$$\frac{\partial U}{\partial t} + U\frac{\partial U}{\partial x} + V\frac{\partial U}{\partial y} = -\frac{1}{\rho}\frac{\partial P}{\partial x} + \nu\left(\frac{\partial^2 U}{\partial x^2} + \frac{\partial^2 U}{\partial y^2}\right) \ , \tag{2}$$

$$\frac{\partial V}{\partial t} + U\frac{\partial V}{\partial x} + V\frac{\partial V}{\partial y} = -\frac{1}{\rho}\frac{\partial P}{\partial y} + \nu\left(\frac{\partial^2 V}{\partial x^2} + \frac{\partial^2 V}{\partial y^2}\right) \quad , \tag{3}$$

respectively. The appropriate initial (i.e. t=0) and boundary conditions are:

$t=0: \quad U = V = 0$

$t>0: \quad U = V = 0$ at plain plate walls

$U = U_{in}, V = 0$ at the inlet, i.e. x=0

$\frac{\partial U}{\partial x} = 0, \frac{\partial V}{\partial x} = 0$ at x=B

$U = V = 0$ at y=0 and W, i.e. at channel wall.

In reference to the finite difference methods proposed by Harlow and Welch (1965) and Hirt *et al.* (1975), the governing equations can be discretized as:

$$U_{i,j}^{n+1} = U_{i,j}^{n} + \Delta t\left[\frac{1}{\Delta x}\left(P_{i,j}^{n} - P_{i+1,j}^{n}\right) - FUX^{n} - FUY^{n} + VISX^{n}\right] \tag{4}$$

$$V_{i,j}^{n+1} = V_{i,j}^{n} + \Delta t\left[\frac{1}{\Delta Y}\left(P_{i,j}^{n} - P_{i,j+1}^{n}\right) - FVX^{n} - FVY^{n} + VISY^{n}\right] \tag{5}$$

Here, the P terms in equations (4) and (5) include ρ. Figure 3 depicts an arrangement of finite difference variables for a typical cell. The subscripts and superscripts correspond to the cell location and time instant, respectively. Thus, $P_{i,j}^{n}$ denotes the pressure at the center of a cell (i,j) at the time instant n. $U_{i,j}^{n}$ and $V_{i,j}^{n}$ denote the x- and y-direction velocity components at the middle of the right and top sides of the cell (i,j), respectively, at the time instant n. FUX^{n}, FUY^{n}, $VISX^{n}$, FVX^{n}, FVY^{n}, and $VISY^{n}$ (Hirt *et al.* 1975) are defined as

$$FUX^{n} = \frac{1}{4\Delta X}\left[\left(U_{i,j}^{n} + U_{i+1,j}^{n}\right)^2 + \alpha\left|U_{i,j}^{n} + U_{i+1,j}^{n}\right|\left(U_{i,j}^{n} - U_{i+1,j}^{n}\right) - \left(U_{i-1,j}^{n} + U_{i,j}^{n}\right)^2 - \alpha\left|U_{i-1,j}^{n} + U_{i,j}^{n}\right|\left(U_{i-1,j}^{n} - U_{i,j}^{n}\right)\right] \tag{6}$$

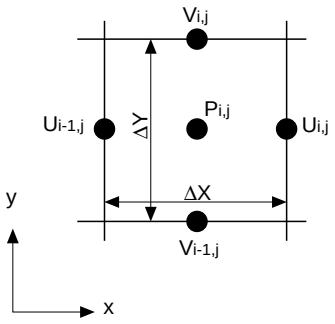

Figure 3.
Arrangement of finite difference variables in a typical cell

$$FUY^n = \frac{1}{4\Delta Y}\Big[(V^n_{i,j} + V^n_{i+1,j})(U^n_{i,j} + U^n_{i,j+1}) + \alpha|V^n_{i,j} + v^n_{i+1,j}|(U^n_{i,j} - U^n_{i,j+1}) - (V^n_{i,j-1} + V^n_{i+1,j-1})(U^n_{i,j-1} + U^n_{i,j}) - \alpha|V^n_{i,j-1} + V^n_{i+1,j-1}|(U^n_{i,j-1} - U^n_{i,j})\Big] \quad (7)$$

$$VISX^n = \nu\Big[\frac{1}{\Delta X^2}(U^n_{i+1,j} - 2U^n_{i,j} + U^n_{i-1,j}) + \frac{1}{\Delta Y^2}(U^n_{i,j+1} - 2U^n_{i,j} + U^n_{i,j-1})\Big] \quad (8)$$

$$FVX^n = \frac{1}{4\Delta X}\Big[(U^n_{i,j} + U^n_{i,j+1})(V^n_{i,j} + V^n_{i+1,j}) + \alpha|U^n_{i,j} + U^n_{i,j+1}|(V^n_{i,j} - V^n_{i+1,j}) - (U^n_{i-1,j} + U^n_{i-1,j+1})(V^n_{i-1,j} + V^n_{i,j}) - \alpha|U^n_{i-1,j} + U^n_{i-1,j+1}|(V^n_{i-1,j} - V^n_{i,j})\Big] \quad (9)$$

$$FVY^n = \frac{1}{4\Delta Y}\Big[(V^n_{i,j} + V^n_{i,j+1})^2 + \alpha|V^n_{i,j} + v^n_{i,j+1}|(V^n_{i,j} - V^n_{i,j+1}) - (V^n_{i,j-1} + V^n_{i,j})^2 - \alpha|V^n_{i,j-1} + V^n_{i,j}|(V^n_{i,j-1} - V^n_{i,j})\Big] \quad (10)$$

$$VISY^n = \nu\Big[\frac{1}{\Delta X^2}(V^n_{i+1,j} - 2V^n_{i,j} + V^n_{i-1,j}) + \frac{1}{\Delta Y^2}(V^n_{i,j+1} - 2V^n_{i,j} + V^n_{i,j-1})\Big] \quad (11)$$

The nondimensional factor α in each equation is a weight coefficient. α=0.5 is employed in the present study.

The system variables P, U and V are calculated with a staggered grid as proposed by Harlow and Welch (1965). When the grid system is changed from 20×80 to 80×320, a computation reveals only a small difference, that is, the maximum difference is under 1 per cent. Hence, a grid system of 20×80 nodal points with uniformly distributed nodal points is employed to save computation time. Computations proceed in the following order:

(1) Specify the initial values of U and V at zero sec and assign a pressure.

(2) Solve equations (4) and (5) for U and V, subject to the appropriate boundary conditions.

(3) Calculate pressure change for each cell using the equation.

$$\delta P = - \frac{\frac{1}{\Delta X}(U_{i,j} - U_{i-1,j}) + \frac{1}{\Delta Y}(V_{i,j} - V_{i,j-1})}{\left\{2\Delta t\left(\frac{1}{\Delta X^2} + \frac{1}{\Delta Y^2}\right)\right\}} . \quad (12)$$

This is followed by evaluating each velocity component and pressure using

$$U_{i,j}^{(k+1)} = U_{i,j}^{(k)} + \frac{\Delta t \delta P^{(k)}}{\Delta X} \quad (13)$$

$$U_{i-1,j}^{(k+1)} = U_{i-1,j}^{(k)} - \frac{\Delta t \delta P^{(k)}}{\Delta X} \quad (14)$$

$$V_{i,j}^{(k+1)} = V_{i,j}^{(k)} + \frac{\Delta t \delta P^{(k)}}{\Delta Y} \quad (15)$$

$$V_{i,j-1}^{(k+1)} = U_{i,j-1}^{(k)} - \frac{\Delta t \delta P^{(k)}}{\Delta Y} \quad (16)$$

$$P_{i,j}^{(k+1)} = P_{i,j}^{(k)} + \delta P^{(k)} \quad (17)$$

where the superscripts k and k+1 signify two successive iterations.

(4) Repeat steps 2 and 3 until mass conservation for each cell is satisfied under the criterion of

$$\frac{1}{\Delta X}(U_{i,j} - U_{i-1,j}) + \frac{1}{\Delta Y}(V_{i,j} - V_{i,j-1}) \leq 10^{-3} \quad (18)$$

followed by evaluating the convergent values of U and V. Note that if the criteria for convergence is over 10^{-3}, the computation is found to become unstable in the preliminary calculation.

(5) Repeat steps 2 through 4 until t reaches a prescribed time, say, t=3000 sec after the calculation is initiated.

Numerical computation was performed on a Fujitsu personal computer (Pentium Pro CPU 200MHz) at time interval $\Delta t=0.0001$ sec which consumed up to 24 CPU hours, using water as the working fluid (Pr=7.1). The Reynolds number (Re) ranges from 4 to 280. L/δ is fixed at 2.5 while d/δ is varied from 2.0 to 6.0. Notice that the channel width, W, is large enough that it has no affect on the flow pattern over the perforated plates.

Results and discussion

Figure 4, for Re=4 and $d/\delta=2.0$, depicts the timewise variation of flow patterns over both sides of the single-slot perforated plate. Notice that velocity components are normalized by dividing it by inlet velocity. Consecutive images in Figure 4 are obtained at a time interval of 10.0 sec. It is observed that the fluid flows straight downstream as if the slot was not present. However, as the Reynolds number is increased to 280, one observes both a recirculation zone at the wake region of each plate with the flow dipping into the slot from both sides and the alternating change in the fluid flow downstream from the rear plate, as seen in Figure 5. The flow

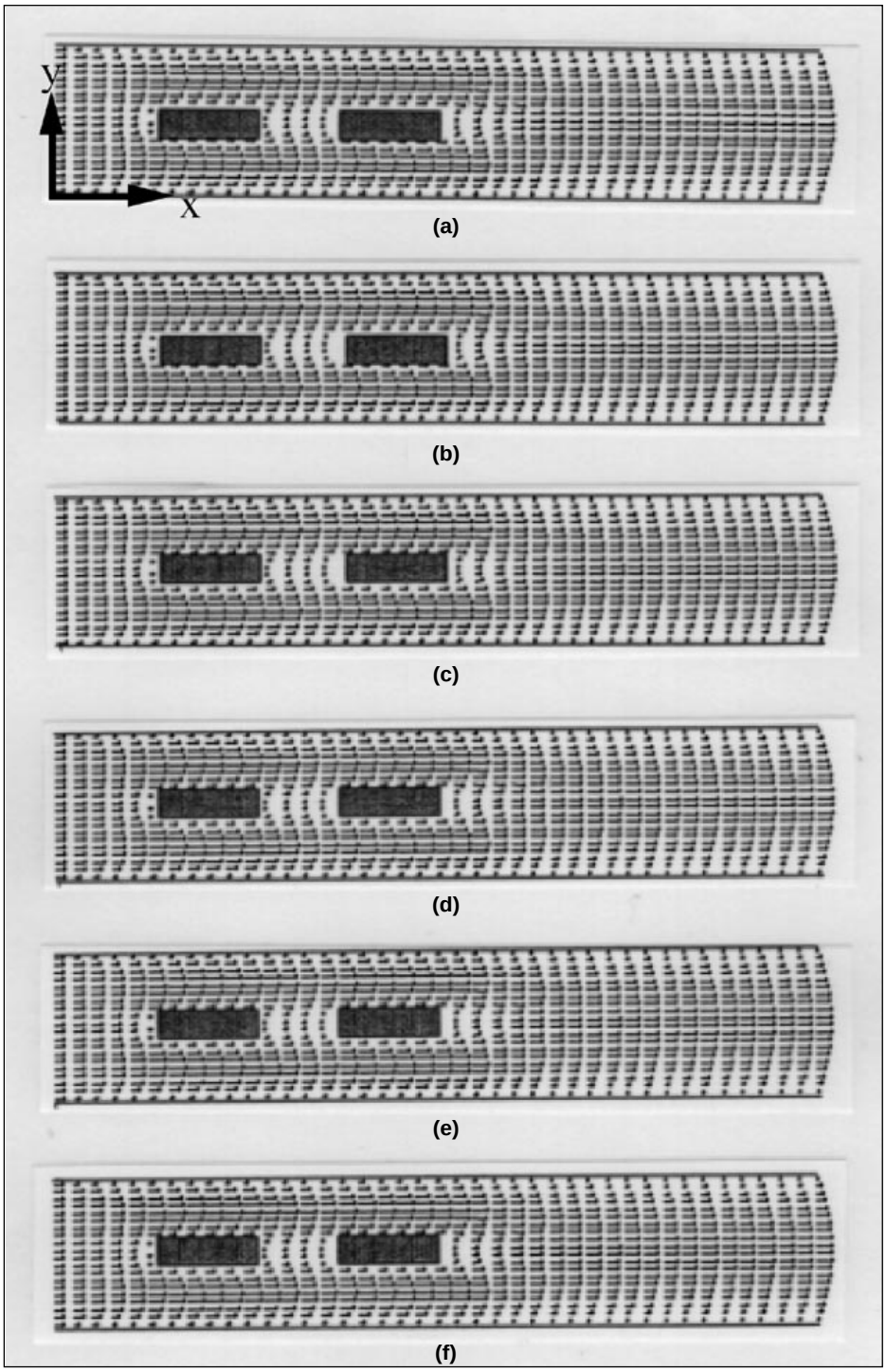

Figure 4.
Timewise variation of velocity-vector field around the perforated plate at a time interval of t=10.0 sec., for Re=4 and $d/\delta=2.0$

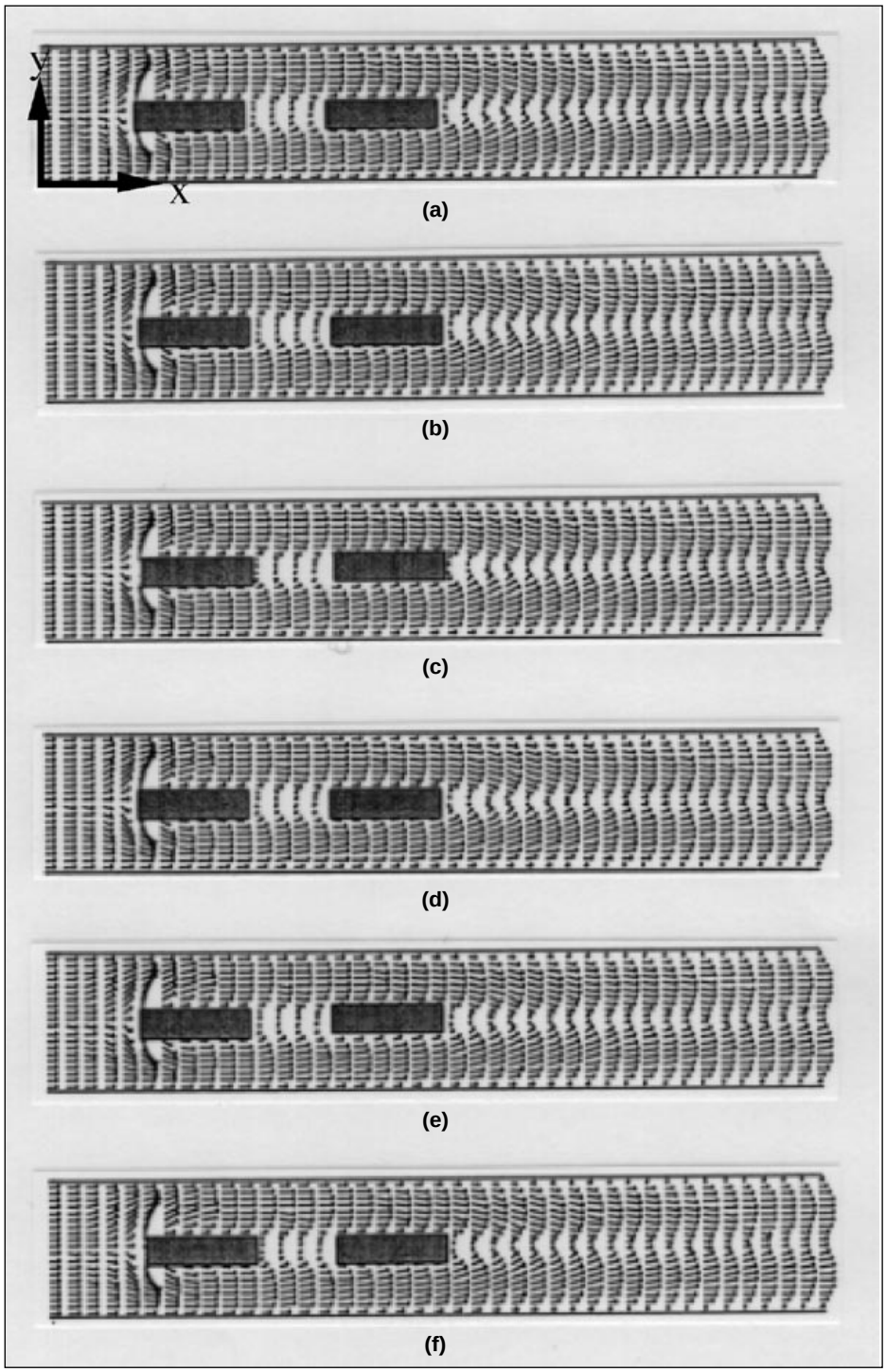

Figure 5.
Timewise variation of velocity-vector field around the perforated plate at a time interval of t=10.0 sec., for Re = 280 and d/δ=2.0

characteristics between two plates is in accordance with the still photograph and its sketch of flow patterns in Figure 6. These flow patterns in Figures 4 and 5 remain steady as evidenced by the absence of temporal variation in the velocity vector.

Figure 7 depicts a sequence of alternating crossing of flow streaklines from one side of the plate to the other through the slot when d/δ reaches 4. The corresponding still photograph and the sketch of the flow pattern are shown in Figure 8. Here, the Reynolds number is the same as that in Figure 5. An alternating change in the flow direction near the lower lip of the slot results in the vibration of flow streaklines across the slot. This, in turn, promotes mixing of the upper and lower streams of the plate downstream from the slot. The predicted alternating change in the fluid flow across the slot is in accord with the still image seen in Figure 8. With the Reynolds number fixed at Re=280, an enlargement in the slot length d results in an enhancement in the fluctuation of flow streaklines with the generation of a recirculation zone between at the front tip of the rear plate and the lower lip of the slot, as seen in Figure 9 for $d/\delta=6.0$.

One may group the flow patterns observed in Figures 4 to 9 into four categories A, B, C and D as schematically depicted in Figure 10. The existence of these four flow patterns was reported by Liang (1975) and Torii and Yang (1998). Since each category is determined by Re and d/δ, a flow pattern map may be constructed by combining these two variables, as listed in Figure 11. It is seen that the alternating crossing at fluid streams (i.e. vibration of flow streaklines across the slot) occurs only in categories C and D, with d/δ over 4.0 and Re exceeding 200. Flow category C occurs when d/δ is in the range of 4.0 to 5.5, beyond which flow category D takes place. In the experiment by Liang (1975) for a single-plate-single-slot and in the numerical study by Torii and Yang (1998) for a slot-perforated flat surface in free stream, the alternating cross-over of fluid streams was found to begin at $d/\delta=2.0$ and 2.5, respectively.

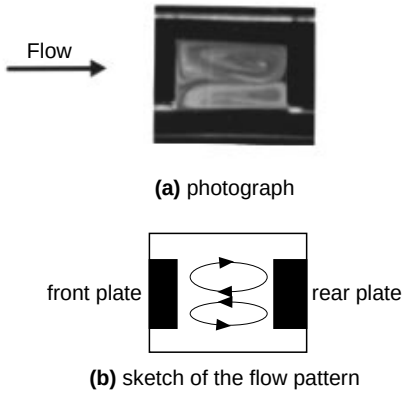

(a) photograph

(b) sketch of the flow pattern

Figure 6.
Visualization of streamline between two plates for Re=280 and $d/\delta=2.0$

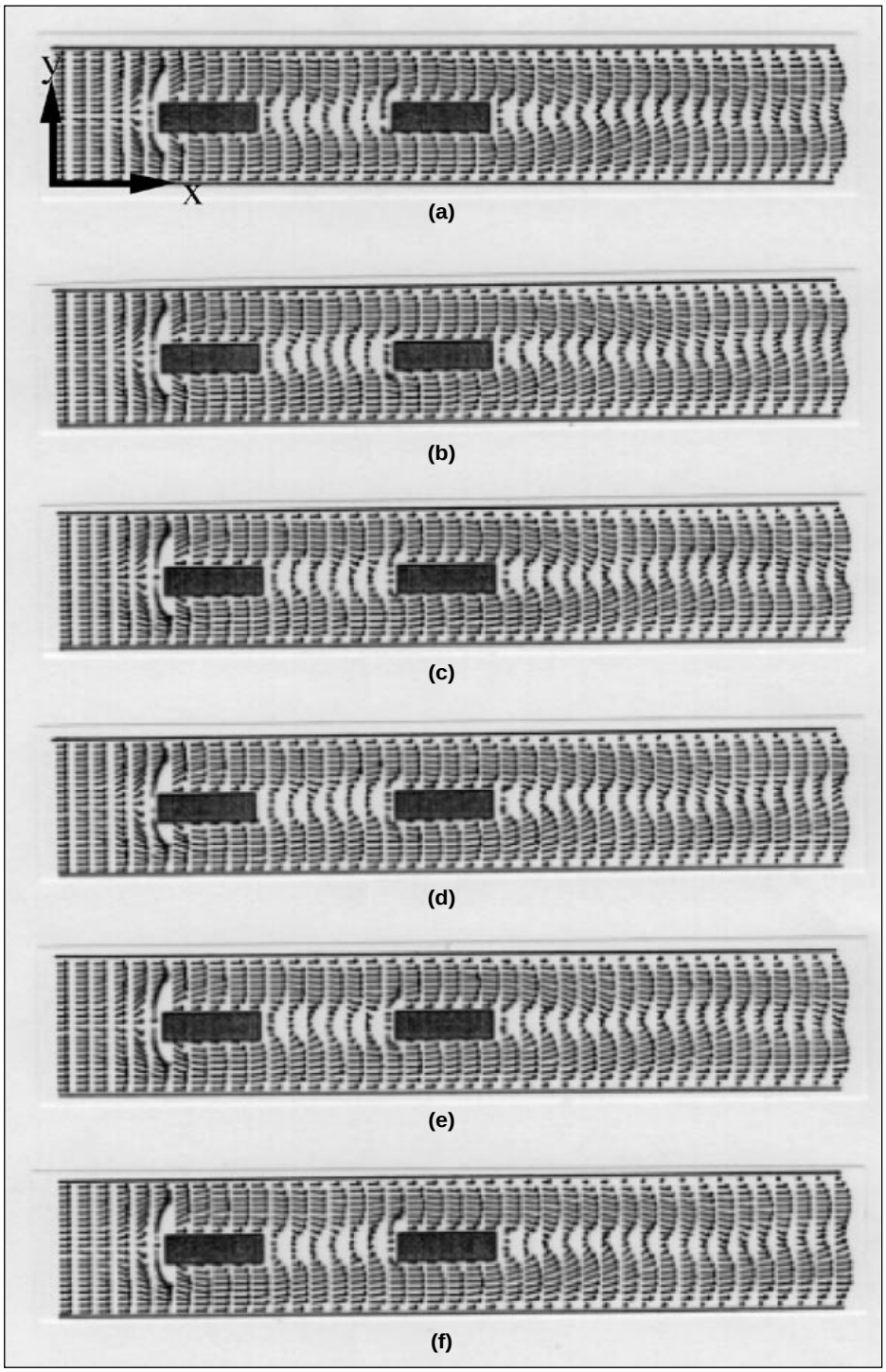

Figure 7.
Timewise variation of velocity-vector field around the perforated plate at a time interval of t=10.0 sec., for Re=280 and d/δ=4.0

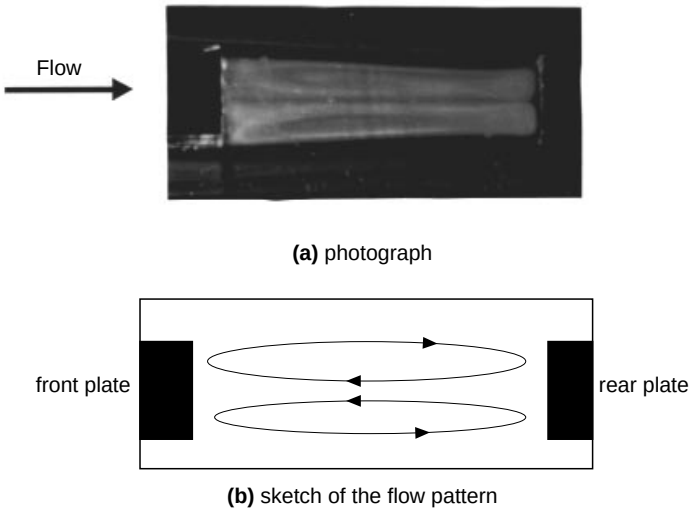

(a) photograph

(b) sketch of the flow pattern

Figure 8.
Visualization of streamline between two plates for Re=280 and d/δ=4.0

These values are slightly less than 4.0, determined by the numerical analysis. It is postulated that the difference is due to the onset of vibration of flow streaklines across the slot being suppressed by the presence of the channel wall. The value of d/δ=4.0 represents the critical ratio below which flow crossing in the slot never occurs regardless of increases in the Reynolds number. For any value of d, category A occurs in a very low Reynolds number region and the dip-in flow pattern, category B, extends over substantially broad ranges of Re as well as d/δ. Flow pattern map of categories A and B is similar to the case of flow over a slot-perforated flat surface in free stream (Torii and Yang, 1998).

Summary

A numerical and experimental study has been performed on unsteady fluid flow over a perforated plate (consisting of two plates spaced at an interval of d in the flow direction) installed in a channel. The roles of the Reynolds number, Re, and the ratio of the slot width, d, to the plate thickness, δ, on the flow field have been investigated.

It is disclosed that flow patterns between two plates may be classified into four categories through a combination of Re and d/δ. At a certain combination of Re and d/δ, an alternating crossing of flow of the fluid streams takes place through the slot from one side to the other side of the plate. A flow pattern map has been constructed to define the range of four different flow categories. The validity of numerical results has been confirmed through experimental flow visualization.

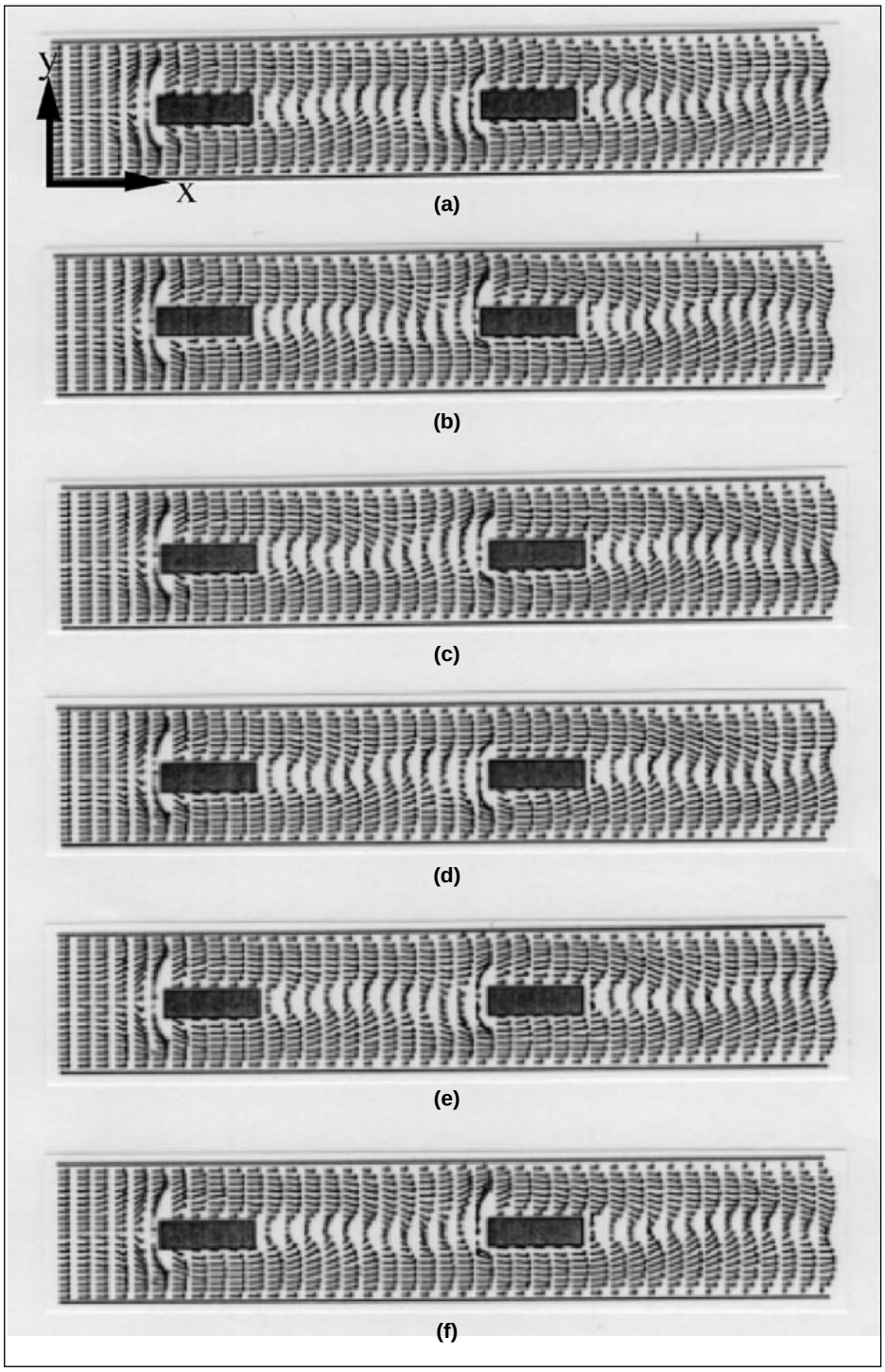

Figure 9.
Timewise variation of velocity-vector field around the perforated plate at a time interval of t=10.0 sec., for Re=280 and d/δ=6.0

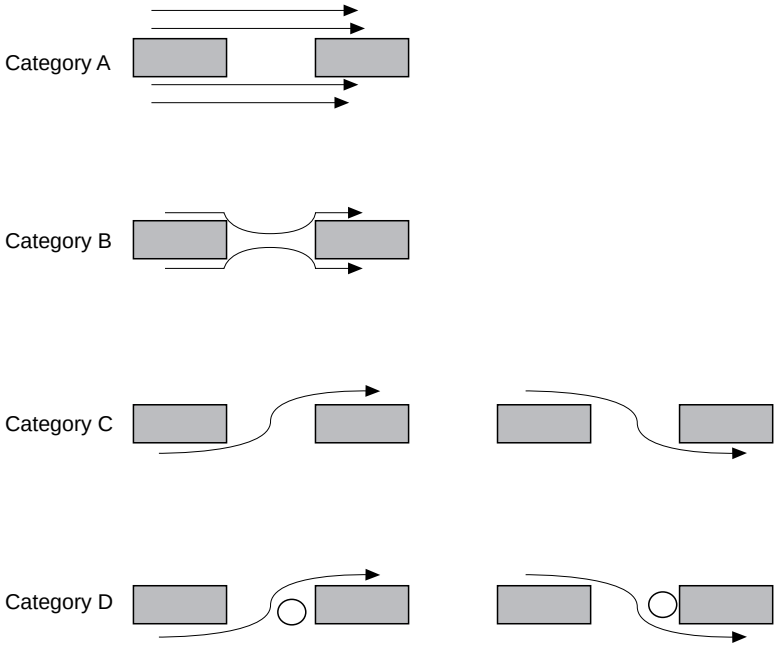

Figure 10.
Classification of flow patterns on a perforated plate

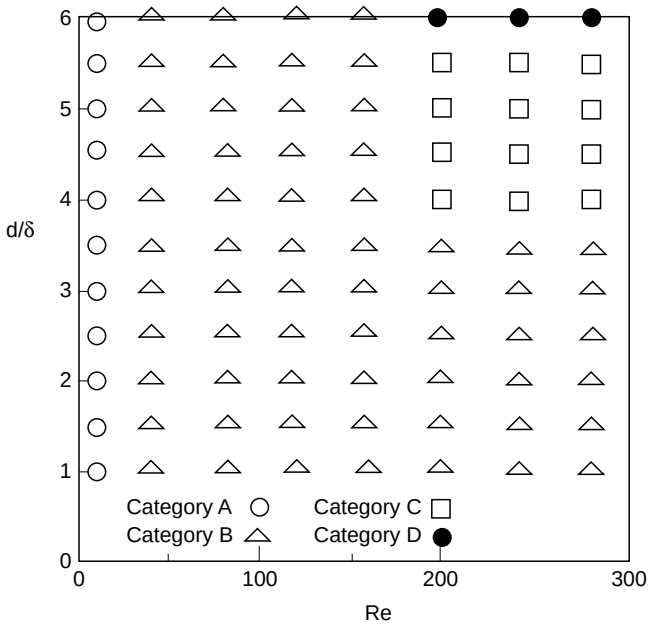

Figure 11.
Flow pattern map

References

Fleming, R.B. (1969), "A compact perforated-plate heat exchanger", *Advances in Cryogenic Engineering*, Vol. 14, Plenum, pp. 197-204.

Fujii, M., Seshimo, S. and Yamanaka, G. (1988), "Heat transfer and pressure drop of perforated surface heat exchanger with passage enlargement and contraction", *International Journal of Heat Mass Transfer,* Vol. 31 No. 1, pp. 135-42.

Harlow, F.H. and Welch, E.J. (1965), "Numerical calculation of time-dependent viscous incompressible flow of fluid with free surface", *Phys. Fluids,* Vol. 8, pp. 2182-89.

Hirt, C.W., Nichols, B.D. and Romero, N.C. (1975), "SOLA-A numerical solution algorithm for transient fluid flows", LASL Report, LA-5852.

Hwang, G.J., Wu, C. C., Lin, L.C. and Yang, W-J. (1996), "Investigation of flow drag and forced convective heat transfer in perforated coolant channels", *Transport Phenomena in Combustion,* Vol. 2, Taylor & Francis, pp. 1747-58.

Kays, W.M. (1958), "The heat transfer and flow friction characteristics of a wave fin, a strip fin, and a perforated fin heat transfer", No. 39, Dep. Mech. Eng., Stanford Univ., Stanford, CA.

Lee, C.P. and Yang, W-J. (1978), "Augmentation of convective heat transfer from high-porosity perforated surfaces", *Heat Mass Transfer 1978-Toronto,* Vol. 2, pp. 589-94.

Liang, C.Y. (1975), "Heat transfer, flow friction, noise and vibration studies of perforated surface", Ph. D. Thesis, University of Michigan, Ann Arbor, Michigan.

Liang, C.Y. and Yang, W-J. (1975a), "Heat transfer and friction loss performance of perforated heat exchanger surface", *Trans. ASME, Heat Transfer Conf.,* Vol. 97, pp. 9-15.

Liang, C.Y. and Yang, W-J. (1975b), "Modified single blow technique for performance evaluation on heat transfer surface", *Trans. ASME, Heat Transfer Conf.,* Vol. 97, pp. 16-21.

Liang, C.Y. and Yang, W-J. (1975c), "Frequency of vortex shedding, vibration and noise in perforated-plate stacks", *Proc. 12th Annual Meeting of Soc. of Eng, Sci.,* pp. 797-806.

Liang, C.Y., Lee, C.P. and Yang, W-J. (1976), "Visualization of fluid flow past perforated surfaces", *Proc. Japanese 4th Symp. Flow Visualization,* pp. 69-73.

Liang, C.Y., Yang, W-J. and Clark, J.A. (1974), "Slotted-fin tubular heat exchangers for dry cooling towers", *ASME Paper,* No. 74-HT-6.

Liang, C.Y., Yang, W-J. and Hung, Y.Y. (1977), "Perforated-fin type compact heat exchangers for gas turbines", *1977 Tokyo Joint Gas Turbine Congress,* pp. 77-85.

McMahon, H.O., Brown, R.J. and Bleyle, G.A. (1950), "A perforated-plate heat exchanger", *Trans. ASME,* Vol. 72, pp. 623-33.

Shah, R.H. and Osborn, H.H. (1967), "Final report-advanced heat exchanger design of compact heat exchanger when operating in a marine environment", Air Preheat Company, Wellesville, New York, NY.

Siegla, D.C. (1972), "Heat transfer and friction behavior of perforated plate fin surface intended for gas turbine recuperators", Internal Report, General Motors Research Lab., Warren, MI.

Torii, S. and Yang, W-J. (1998), "Numerical flow visualization of a slot-perforated flat surface in free stream", *Proceedings CSME FORUM 1998,* Vol. 1, pp. 177-84.

Vonk, G. (1968), "A new type of compact heat exchanger with a high thermal efficiency", *Advances in Cryogenic Engineering,* Vol. 13, Plenum, pp. 582-9.

Wong, S., Duncan, J.D., Gibson, J.C. and Killackey, J.J. (1971), "Compact condenser for rankine cycle engine", Final Report 71-7464, (Prepared for Environmental Protection Agency), Air Research Manufacturing Co., CA.